Article:

eprints@whiterose.ac.uk
https://eprints.whiterose.ac.uk/

An Ultrasonic Method for Measurement of Oil Films in Reciprocating Rubber O-ring Seals

Juanjuan Zhu [a], Xiangwei Li [a*], Scott Beamish [a], Rob S Dwyer-Joyce [a]

[a] The Leonardo Centre for Tribology, Department of Mechanical Engineering, University of Sheffield, Mappin Street, Sheffield, S1 3JD, UK
[*] Corresponding Author: Dr Xiangwei Li, lixwvigour@hotmail.com; xiangwei.li@sheffield.ac.uk

Abstract

In this study, ultrasound has been developed and applied for a rubber O-ring subjected to reciprocating sliding. Under varying reciprocating speeds (2-8 Hz) and normal loads (10-20 N), ultrasonic reflection from the sealing contact was measured for analyzing the oil film formation. Central film thickness measurements were found to be in the range of 1.8-7 μm, which were comparable to the modelling results. Contact sizes measured experimentally were slightly larger than predicted by Hertzian theory. In addition, the oil film along the reciprocating path was measured using an array of ultrasound sensors; this mapped the oil film formation covering the length of the reciprocating stroke. The findings have concluded that the ultrasound technique is an effective approach in detecting the oil film formation and contact size for the sealing contact.

Keywords: reciprocating seal, electrohydrodynamic lubrication, ultrasound method, oil film

1. Introduction

The reciprocating seals in hydraulic actuators are usually soft, non-metallic rings fixed in grooves to block or separate fluid in reciprocating motion applications. They are critical machine elements that provide a way for fluid power to be converted to linear motion. They are designed to prevent leakage of a lubricant or sealed media and ensure efficient and safe operation of hydraulic systems. They are present in almost all aspects of automobile, aerospace, marine, and wider manufacturing sectors [1-3]. Hydraulic reciprocating seals encompass rod seals and piston seals. Rod seals are exposed to the motion on their inner diameter along the rod of a hydraulic cylinder, piston seals are exposed to the motion on their outer diameter along the bore of a hydraulic cylinder.

Reciprocating seals function by allowing the formation of a thin film of liquid at the interface between the seal and the rod. This prevents direct rubbing of the seal lip against the rod or cylinder. Friction and wear are thus minimized. Lubricated by this thin oil layer, reciprocating seals work as a barrier preventing the leakage of the sealed liquid. If the film is too thin solid contact, wear, and failure can result. If the film is too thick then excessive leakage occurs, leading to a loss in hydraulic efficiency and environmental hazard. Understanding seal behavior is challenging because there are a large number of variables that affect performance [4], such as seal geometric profile, roughness, tolerances, sealed pressures, sliding speeds, and temperatures. In addition, reciprocating seals are usually soft non-metallic materials, such as polyurethane, rubber, or PTFE and their compounds with fiber reinforcements. This means that their mechanical properties are complex, following non-linear elastic stress-strain laws. In addition, the elastic modulus, hardness, and compressibility are sensitive to environment, such as temperature and humidity. This inevitably brings extra difficulty in evaluating the behavior of the reciprocating seals in practical applications.

Evaluation of reciprocating seal performance from experimental work can be traced back to 1940s, mainly dealing with the issues of lubrication, leakage, and friction [5-7]. In the past 20

years, thanks to sensing technique developments, the contact film thickness [8-10], seal frictional force [11-12], contact pressure distribution and size [13-14], and the leakage [15-16] have been widely studied using optical interferometry, electrical sensors [17-20] and acoustic emission approaches [21]. However, certain approximations and simplifications must be made in order to facilitate the execution of those evaluation techniques. For example, unavoidable background noise has been hindering the application of acoustic emission method in industrial machines. In using the optical interferometry approach, transparent plastic tubes were adopted to replace the metal rod [14, 22-23]; these possesses different mechanical and physical properties, e.g., roughness, asperity dimension and distribution, elastic deformation behaviors etc. In addition, due to the poor reflection of rubber surfaces, either the seal surface was covered by an aluminized, thin, plastic-sheet [24], or coated with gold layer to improve reflectivity [25], which altered the real surface microtopography.

Recent theoretical simulations, e.g., by analytical tools and Finite Element Analysis [26], have been widely carried out thanks to improved computational capacity, predicting leakage, friction force and contact pressure [27]. However, these key issues remain very much a concern today, although advanced experimental techniques and improved computational capacity narrow the gap between simulation simplifications and real operating conditions.

Recently developed ultrasonic methods have been used for monitoring tribological contacts, including lubricant film thickness [28-30], contact pressure and size [31] and friction [32]. These provide a promising approach for inspecting the hydraulic reciprocating seal without modification to the sealing structures. Ultrasonic trials have been conducted by Reddyhoff et al. [33-34] for measuring lubricant film thickness in the mechanical face seals made from stiff ceramics. Ultrasound does not transmit well through elastomers, and metal-elastomer contacts are acoustically mismatched. This has hampered the use of ultrasound in seal type contacts. The only contrition to date has been from Gasni et al [35] who studied elastomer contacts on Perspex in a simple rolling experiment. However, the geometry, kinematics, and complex materials make this a challenging application for an ultrasonic sensor. In this study, these challenges have been overcome to develop an ultrasound method on a model reciprocating nitrile rubber O-ring seal.

2. Background

2.1 Elastomer seal contact and lubrication

Lubricated contacts that involve low modulus materials do not generate sufficient pressure to cause an increase in liquid viscosity but are of a magnitude that produce elastic deformation at least comparable to film thicknesses. This regime of lubrication is known as isoviscous elastohydrodynamic lubrication (EHL) [35-36] or commonly, yet somewhat erroneously, soft EHL. For contacts with high modulus materials (e.g., gear teeth and rolling element bearings) [37-38], modelling based on the Reynolds equation and elastic deformations is well established and there are plenty of methods for the prediction of fluid film thickness and pressure distribution. For materials of low elastic modulus, the investigation of their contacts has been sparse in literature. In analyzing the lubricant film thickness for this type of contact, e.g., between rubber seal and metal rod, the widely used analysis has been the Hamrock and Dowson [39] model,

$$\overline{H_c} = 7.32 \times \left(1 - 0.72 \times e^{-0.28k}\right) \times \overline{U}^{0.64} \times \overline{W}^{-0.22} \tag{1}$$

Dimensionless parameters are defined as: dimensionless film thickness, $\overline{H_c} = \frac{h_c}{R'_x}$,

dimensionless speed parameter, $\overline{U} = \frac{\eta_0 \times u}{E' \times R'_x}$, dimensionless load parameter, $\overline{W} = \frac{P}{E' \times R_x'^2}$,

while k is the ellipticity parameter, which is 1 for a circular point contact and 12 when the configuration approaches a line contact (i.e. a reciprocating seal contact [40]), h_c is the central film thickness, R'_x is the reduced radius in the entrainment direction, calculated by $\frac{1}{R'_x} = \frac{1}{r_{1x}} + \frac{1}{r_{2x}}$, r_{1x} and r_{2x} are the radius of two contacting bodies in the entrainment direction, η_0 is the viscosity at the contact inlet, u is the mean surface velocity in the entrainment direction, $u = (u_1 + u_2)/2$, P is the normal load, E' is the reduced elastic modulus and defined by $\frac{2}{E'} = \frac{1-v_1^2}{E_1} + \frac{1-v_1^2}{E_2}$, u_1, u_2, E_1, E_2, v_1, and v_2 are velocity, elastic modulus and Poisson's ratio of the two contacting bodies.

Starting from elliptical contact analysis, based on the work of Hamrock and Dowson [39], Crook [41], and Kanters [40], Nijenbanning et al. [42] derived central lubricant film thickness equations for the line contact of elastomeric seals based on Moes' work [43],

$$H_c = C(D) \times M^{-2/15} \tag{2}$$

$$C(D) = 3.18 \times \left(1 + 0.06 \times ln(D) + 0.63 \times D^{4/7}\right)^{-14/25} \times D^{-1/15} \tag{3}$$

Moes' dimensionless film thickness, $H_c = \frac{h_c}{R'} \times \left(\frac{E' \times R'}{\eta_0 \times u_s}\right)^{1/2}$, Moes' dimensionless load

parameter, $M = \frac{W}{E' \times R'} \times \left(\frac{E' \times R'}{\eta_0 \times u_s}\right)^{1/2}$, while R is the reduced radius of contacting surfaces, $\frac{1}{R'} = \frac{1}{r_{1x}} + \frac{1}{r_{2x}} + \frac{1}{r_{1y}} + \frac{1}{r_{2x}}$, u_s is the sum velocity, $u_s = u_1 + u_2$, D is the ratio of reduced radii, $D = R'_x / R'_y$, $\frac{1}{R'_y} = \frac{1}{r_{1y}} + \frac{1}{r_{2y}}$. In this work, both the Hamrock and Dowson model and the Nijenbanning et al. model have been used for simulating the oil film thickness of the reciprocating rubber O-ring contact to compare with experiment.

2.2 Ultrasonic response from sealing contact

When the ultrasound signal is incident at an interface between two materials, some of the wave amplitude will be reflected and some transmitted. In the case of the reciprocating sealing contact, sketched in Figure 1, a thin oil layer is formed by the relative sliding and the compressing pressure. When ultrasound is incident at the boundary between the bore surface and the thin oil layer, some waves will be bounce back to the ultrasound sensor. Likewise, there will be some waves reflected from the back boundary between the thin oil layer and the O-ring outer surface. Both boundaries act as reflectors. As the oil layer is very thin, the two reflected waves overlap and cannot be distinguished from each other in the time domain [34]. In this case, the oil film behaves as a single reflector. The proportion of the ultrasound energy reflected from reflected from this thin oil layer known as the reflection coefficient, *R*, will be determined by its stiffness, *K*, expressed by Equation (4), known as the spring model [30, 44].
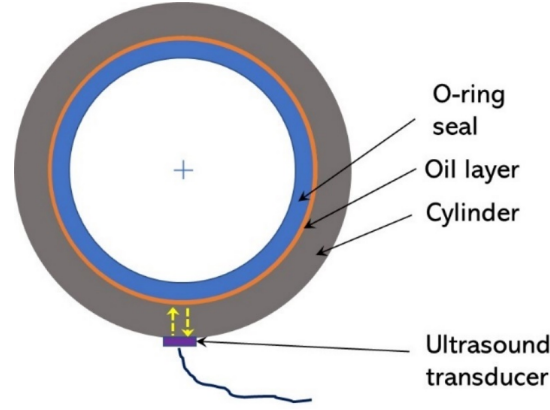
Figure 1. Sketch of the sealing contact between rubber O-ring and a cylinder showing the proposed measurement concept.

$$R = \frac{z_2 - z_1 + i\omega\left(Z_1 Z_2 / K\right)}{z_2 + z_1 + i\omega\left(Z_1 Z_2 / K\right)} \tag{4}$$

where z_1 and z_2 refer to the acoustic impedance of the materials either side of oil layer (acoustic impedance is the product of wave speed and density), which are rubber and cast-iron in this work, ω is the angular frequency of the ultrasound ($\omega = 2\pi f$, f is the frequency). Given an oil bulk modulus of B, the thin oil layer thickness h, is:

$$h = \frac{B}{K} = \frac{\rho c^2}{K} \tag{5}$$

The bulk modulus is the product of the oil density, ρ and square of the speed of sound in the oil, c. Combining Equations (4) and (5), the film thickness is correlated to the reflection coefficient and properties of oil and surrounding layers,

$$h = \frac{\rho c^2}{\omega z_1 z_2} \sqrt{\frac{R^2(z_2 + z_1)^2 - (z_2 - z_1)^2}{1 - R^2}} \tag{6}$$

One of the challenges of this measurement case is that the acoustic impedance of rubber and cast iron are very dissimilar. They are acoustically mismatched and so even if there is no oil film (perfect contact) a large fraction of the wave is reflected; presence of an oil film causes slightly more to be reflected. From Equation (6), it is clear that two materials with a large difference in acoustic impedance, $|z_2 - z_1| / (z_2 + z_1) \to 1$, will lead to $R \to 1$, which means most of the ultrasound wave is reflected, giving the film thickness a value of infinity.

Figure 2 shows a plot of Equation (6) for the case of nitrile butadiene rubber (NBR) against cast iron with a film of oil (using the materials properties of Table 1). The ultrasound reflection between 87 and 99% of the wave amplitude shown in Figure 2 indicates the ideal measurable range. In practice, the ultrasound reflection may be affected by the electromechanical testing and electronic measuring systems, e.g., the electrical noise, system voltage stability, vibration etc.
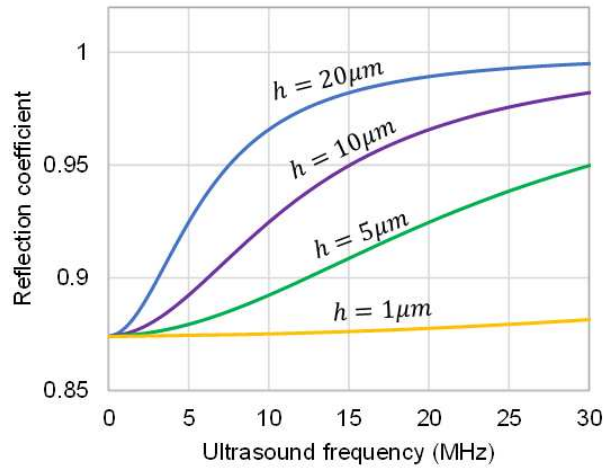
Figure 2. Ultrasound reflection coefficient spectrum for rubber O-ring-oil-cast-iron system for varying oil film thickness as predicted by Equation 6.

In this work, the film thickness generated between a rubber O-ring reciprocating against cast-iron was measured and analysed using Equation (6). Experimental results have been compared with numerical modelling outputs to evaluate the measurement capability.

3. Experimental Method

3.1 Contact configuration and test specimens

In this work, rubber O-rings, shown in Figure 3 (c) with outer diameter of 76 mm and cross-section diameter of 3 mm were tested against a cast-iron plate. Figure 3 (a) shows the sketch of the contact configuration. The rubber O-ring performed reciprocating wiping against a concave cast-iron plate with varying speeds. The normal load, P was applied perpendicular to the sliding direction on the seal via a seal holder. The cast-iron plate acting as the inner surface of a cylinder had a concave curvature of 38 mm.

(a)

(b)

(c)
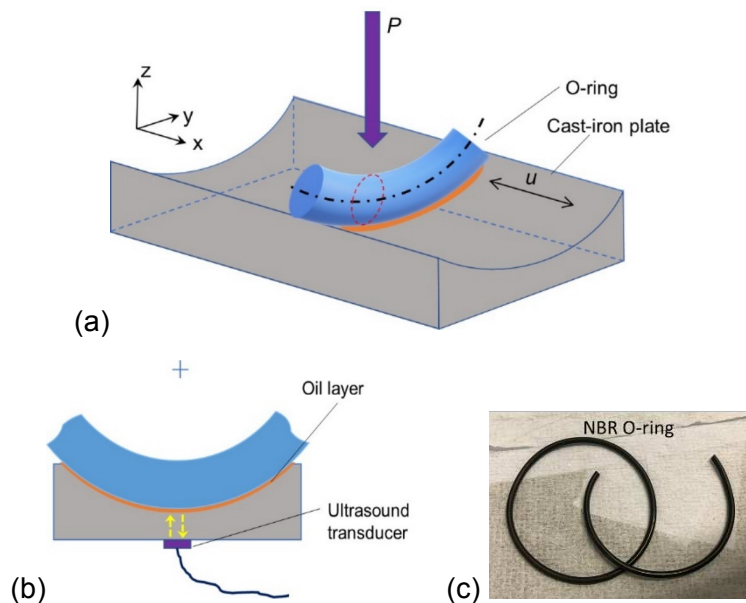
Figure 3. (a) Sketch of contact configuration between rubber O-ring and cast-iron plate, (b) cross-section of the contact perpendicular to the reciprocating direction of the seal, and (c) tested O-ring sample.

The bottom of the plate was flat and instrumented with ultrasound sensors for monitoring the interface during the wiping process of the seal, shown in Figure 3 (b). Prior to the experiment, the outer surface of the O-ring was characterized using an Alicona InfiniteFocusSL microscope (Alicona Imaging GmbH, Graz, Austria), a sample profile is shown in Figure 4. Shell Helix HX5 15W-40 with a kinematic viscosity 106 cst @40°C and 14.27 cst @100°C was used as the lubricant for all conducted tests. The speed of sound of Shell Helix HX5 15W-40 was determined using a chamber of known length (50 mm), instrumented with a 10 MHz longitudinal transducer. Lubricant speed of sound was then be determined by measuring the time between successive ultrasonic reflections. Dimensions, physical and acoustic properties of the tested rubber O-ring and cast-iron plate are listed in Table 1.
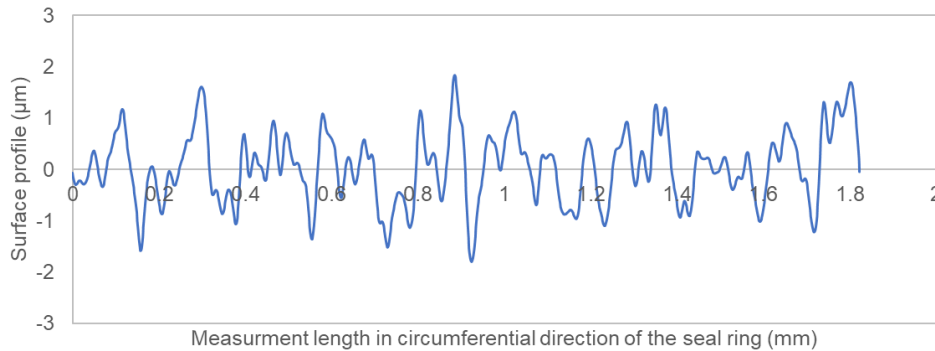
Figure 4. Microscopic surface profile of the rubber O-ring.

Table 1. Dimensions and properties of tested rubber O-ring and cast-iron.

Material	Dimensions	Density, ρ, kg/m^3	Elastic modulus, E, GPa	Poisson's ratio, ν	Ultrasound speed in the material, c, m/s	Acoustic impedance, z, MRayls
NBR O-ring	Inner diameter: 70 mm; cross section diameter: 3 mm	1214	0.00102	0.47	2070 [x]	2.51
Cast-iron	Curvature radius 38mm	7800	106	0.26	4800 [x]	37.44
Shell Helix HX5 15W-40	-	878.7			1460	1.28

3.2 Test apparatus and method

A Plint TE 77 versatile tribometer (Phoenix Tribology Ltd, UK) with a stroke length up to 25 mm and a loading capacity up to 1,000 N was adopted for performing the reciprocating sliding. A normal force is applied via a stirrup-style loading frame, using an inline spring to pull the loading frame onto the reciprocating arm. Figure 5 (a) shows the photos of the test rig and the reciprocating head with the seal sample holder attached. The cast-iron plate was resting in an oil container. Prior to testing, the container was filled with Shell Helix HX5 15W-40 until the plate concave surface was fully immersed. Thus, the contact between the rubber seal and the plate was fully flooded during sliding. An array of 8 longitudinal ultrasound sensors (length × width = 5 × 1.2 mm, 2 mm gap between two sensors) were mounted on the underside of the cast-iron plate as shown in Figure 5 (b), which have a central frequency of 10 MHz. Figure 5 (c) shows the seal sample holder which was attached to the sliding head with a groove to accommodate a length of 20 mm seal section. A fresh seal section was used for each test condition.

Varying normal loads and reciprocating speeds were applied to study their influence on the oil film formation and distribution. A stroke length of 15 mm was adopted, at which the seal was traversed over 5 of the 8 ultrasound sensors (s2 to s6 in Figure 5(b)); readings from those sensors were analyzed.
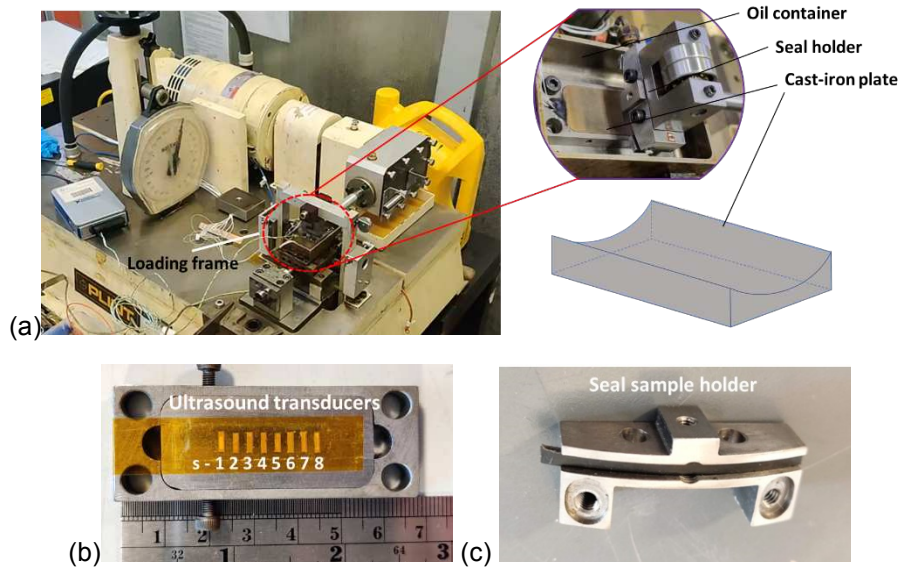
Figure 5. (a) Plint TE77 reciprocating test rig, seal sample holder, (b) ultrasound sensors mounted on the underside of the cast-iron plate, and (c) O-ring seal sample holder.

Table 2 summarizes the test condition used in this work. Normal loads of 10, 15 and 20 N were applied to the seal contact which produced an initial mean Hertzian pressure of 0.38, 0.44 and 0.48 MPa respectively. A 2-minute reciprocating sliding was performed as running-in prior to each measurement. The duration of each test for data collection was kept at around 10 s to consistently avoid the influence from the temperature increase on the sealing material.

Table 2 Test conditions of rubber O-ring sliding against cast-iron.

Normal load, N	Reciprocating frequency, Hz	Stroke length, mm	Engaged sensors	Environment
10, 15, 20	2, 4, 6, 8	15	s2-6	Room temperature (20°C) & humidity

3.3 Measurement system and signal processing

An ultrasonic unit consisting of a high speed ultrasonic pulser and receiver (UPR), a data acquisition analogue module, ultrasound transducers, and a PC for controlling and data processing was adopted for measuring the ultrasonic reflections from the interface. Figure 6 shows the schematic layout of the instrumentation. Along the reciprocating length, each element in the sensor array is labelled as s1 to s8. In measuring, the UPR generates a sequence of short duration voltage pulses that excite the piezoelectric sensor to resonate and send the required ultrasonic pulse through the cast-iron plate. The longitudinal ultrasound sensors with centre frequency 10 MHz were working in pulse-echo mode; the emitter also acts as a receiver. The reflected signal from the lubricant layer on the contact was received by the sensor and amplified by the UPR, which was controlled by the PC using a LabView program.
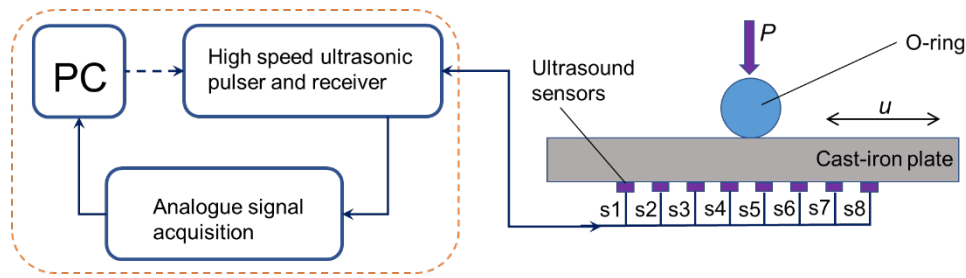
Figure 6. Schematic diagram of the ultrasound measuring instrumentation.

During sliding motion, the rubber O-ring travelled over the inner concave surface of the cast-iron plate. The interface was detected by each sensor as the seal section passed overhead. The ultrasonic reflections were recorded at a data acquisition frequency of 10 kHz in this work.

Figure 7 (a) shows typical reflected signals in the time-domain from the interface with and without the seal located over the sensor. The reflection from the cast-iron plate-air interface is measured and used as the reference signal in the calculation of the ultrasound reflection coefficient. This is because the ultrasound waves are totally reflected from the interface due to the acoustic impedance mismatch between the plate and the air, making the reflection signals equal to the incident signal in amplitude ($R = 1$).

In data processing, a fast Fourier transform (FFT) was performed on the reflected signal, giving amplitude spectrum against frequency, shown in Figure 7 (b). Dividing the reflection signal from lubricant oil film by the reference FFT signal produces the reflection coefficient. This is used for the calculation of oil film thickness using the spring model (Equation (6)).
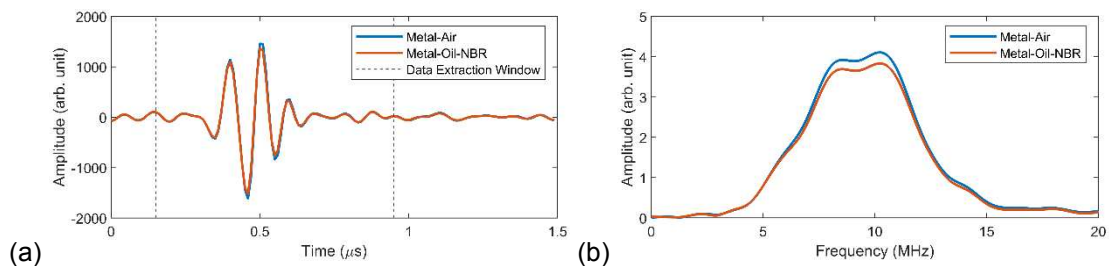
Figure 7. An example of ultrasound signal processing: (a) ultrasound reflected signal in the time domain and data extraction window for FFT transformation; (b) frequency spectrum of reflected ultrasound signal reflection, at 2 Hz reciprocating speed, 20 N normal load, measured by ultrasound sensor s4.

Figure 8 shows an example of the ultrasound signal amplitude, reflection coefficient and oil film thickness for the sliding sealing contact. The periodic amplitude drops in Figure 8 (a) indicate the occurrence of the seal sliding over the sensor. Four passes of the sensor can be seen where the amplitude drops as some of the signal is transmitted into the seal. The reflection coefficient is determined by taking this reflection and dividing by an out of contact reflection (Figure 8(b)). Note how the signal is normally at *R*=1 (the seal is remote from the sensor) and dips down to 0.95 or so when the seal is present. As expected, (from the Figure 2) there is not a great deal of signal change and care has to be taken to reduce electrical noise from the system. Also shown on Figure 8(b) is a signal recorded when the bath is flooded with oil. When the seal is remote form the sensor the reflection occurs at a cast iron to bulk oil interface the coefficient is approximately 0.95. Figure 8 (c) shows the calculated oil film profile for the lubricated case obtained from the spring model (Equation (6)).

8
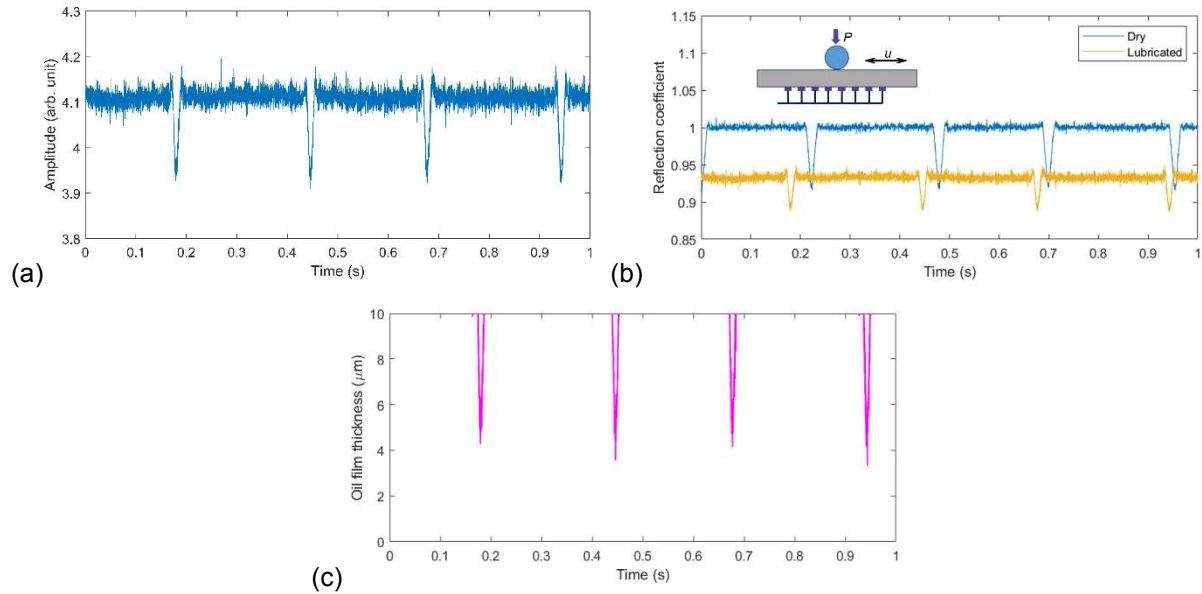
Figure 8. An example of the oil film thickness calculation process: (a) ultrasound reflection amplitude, (b) reflection coefficient, and (c) oil film thickness calculated from (b) using the spring model (Equation (6)). The data was recorded for 2 Hz reciprocating speed, 10 N normal load, and measured by ultrasound sensor s4.

4. Experimental results

4.1 Ultrasound reflection for varying contact conditions

Tests were conducted to study the influence of load and speed on oil film formation. Figures 9-11 show the ultrasound reflection coefficient from sensors s4 (centre stroke), s2, and s6 (stroke ends) for three loads and speeds. Each graph shows a single passage over the sensor. In each case, the reflection coefficient shows a clear reduction in amplitude, while the minimum occurs in the middle of the contact. This is because under normal load and relative sliding, together with the elastic deformation from the seal material, pressure in the lubricant layer builds up while the oil film thickness reduces. Higher pressure causes a stiffer oil layer which facilitates the transmission of the ultrasound signals and therefore causes a reduction ultrasound reflection (Equation (4)).
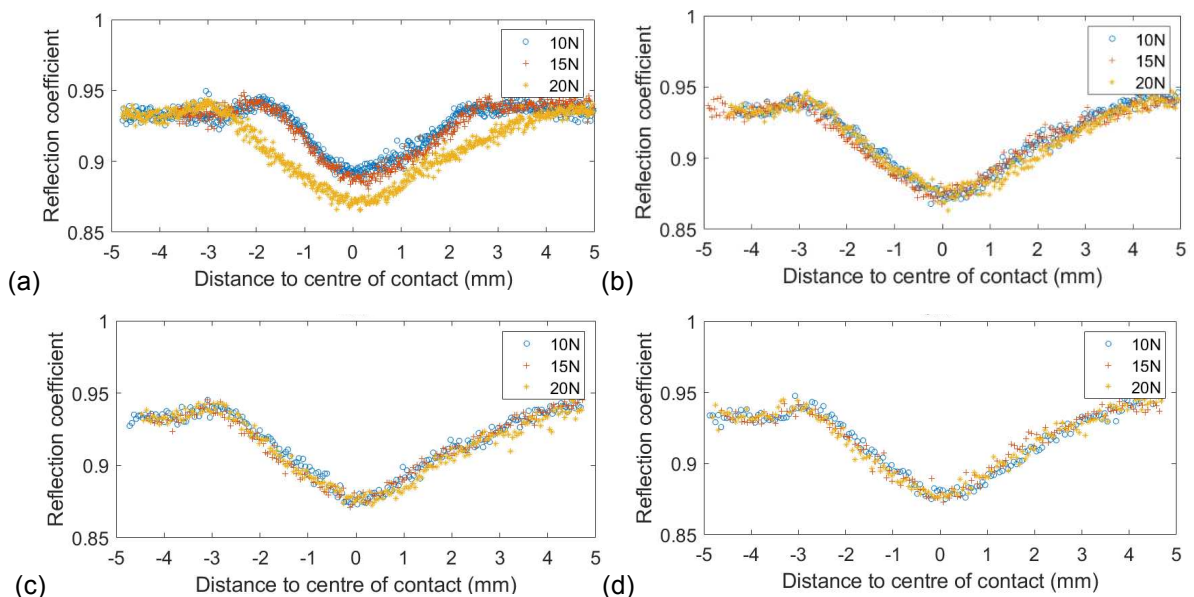
Figure 9. Ultrasound reflection coefficient from the lubricated contact between the NBR O-ring and the cast-iron plate under normal loads of 10, 15, and 20 N, and reciprocating speeds: (a) 2 Hz, (b) 4 Hz, (c) 6 Hz, and (d) 8 Hz, measured by sensor s2 (edge).
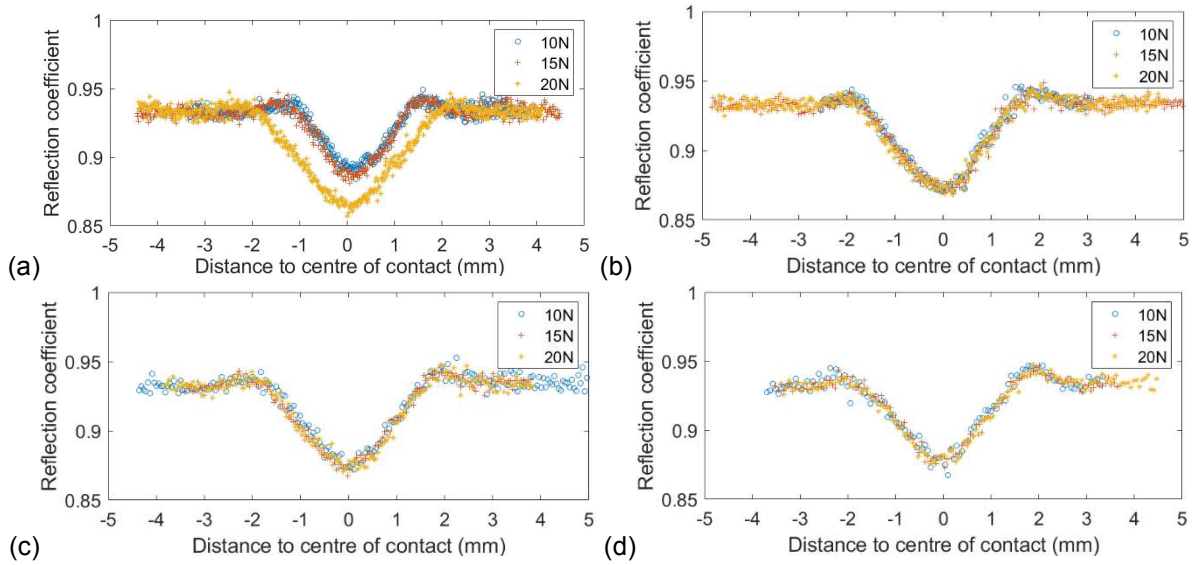
Figure 10. Ultrasound reflection coefficient from the lubricated contact between the NBR O-ring and the cast-iron plate under normal loads of 10, 15, and 20 N, and reciprocating speeds: (a) 2 Hz, (b) 4 Hz, (c) 6 Hz, and (d) 8 Hz, measured by ultrasound sensor s4 (centre).
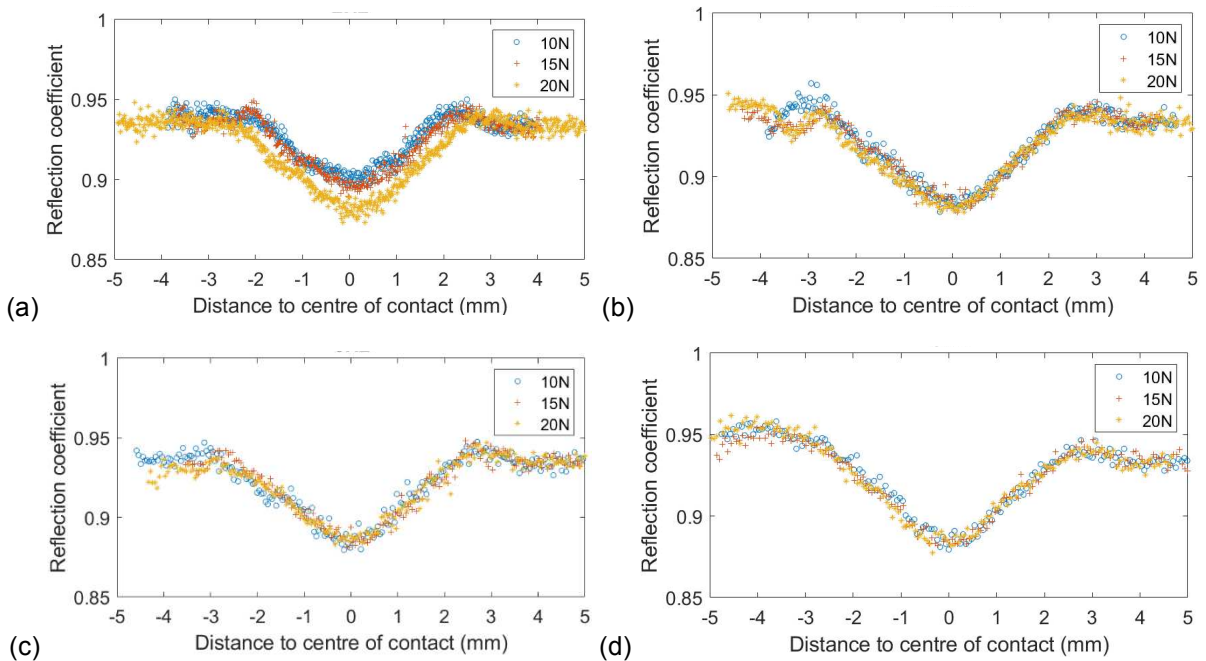
Figure 11. Ultrasound reflection coefficient from the lubricated contact between the NBR O-ring and the cast-iron plate under normal loads of 10, 15, and 20 N, and reciprocating speeds: (a) 2 Hz, (b) 4 Hz, (c) 6 Hz, and (d) 8 Hz, measured by ultrasound sensor s6 (edge).

The profile of the reflection coefficient along the stroke recorded by sensors 2-6 is shown in Figure 12. The increase in normal load has caused a slight increase in the contact width. Based on the sample geometry, Hertzian elliptical contact theory was used to determine the contact size and pressure distribution for each normal load. Figure 12 compares the measured contact width (indicated by reflection coefficient profile) with the Hertzian simulations. Half contact width values from Hertzian theory and ultrasound measurements

10

are presented in Table 3. This shows that experimental measurements indicate a somewhat larger contact than predicted. There are a few reasons for this. Firstly, the sensors are of finite size (1.2 mm width), and this is comparable with the contact size; so, there is some blurring of the sharp edges (note how there is closer agreement for the higher load cases). Secondly, modelling was based on static analysis not considering kinetic effects from the reciprocating contact. And finally, modelling was based on assumptions of perfect smooth surfaces. The interaction of rough surfaces will naturally spread out the contact and the ultrasonic sensors pick this out. Especially when the oil layer thickness is close to the surface roughness (Figure 4), asperity interaction and lubricant layer will be represented by the overall ultrasound reflection, which produces a wider contact width.
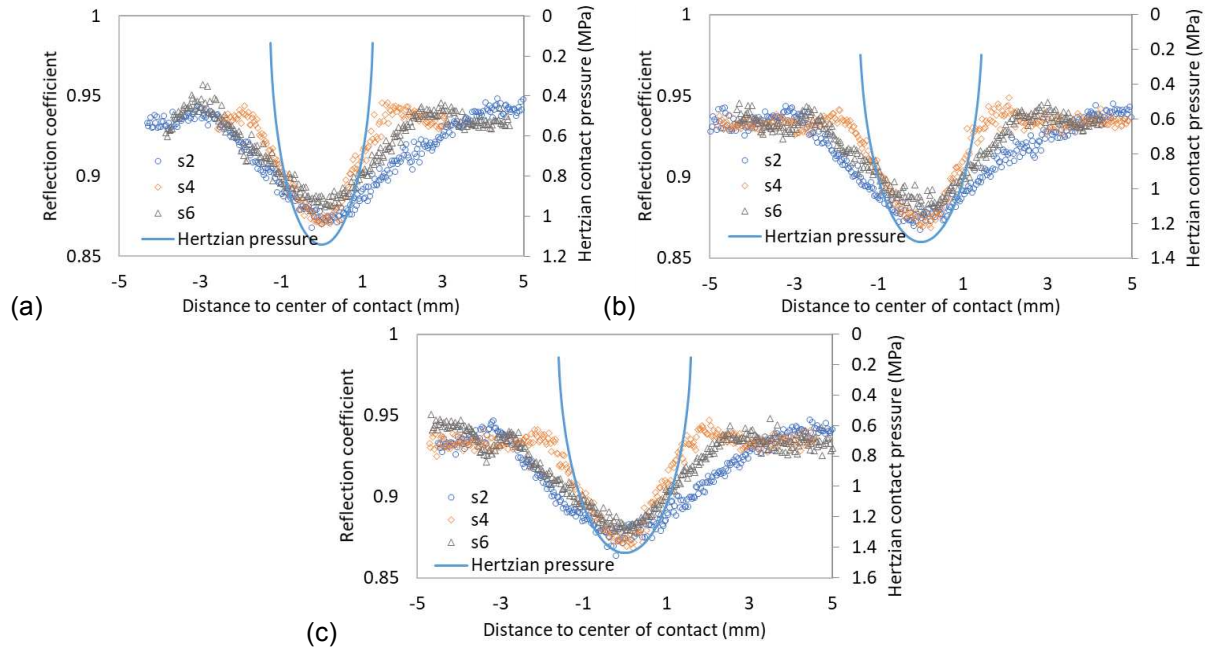
Figure 12. Ultrasound reflection coefficient and Hertzian contact pressure in the contact zone from varying ultrasound sensors under (a) 10 N, (b) 15 N, and (c) 20 N at reciprocating speed of 4 Hz.

Table 3. Half contact width from Hertzian theory and ultrasound measurements.

	@2 Hz, mm			@6 Hz, mm			@8 Hz, mm			
Load, N	s2	s4	s6	s2	s4	s6	s2	s4	s6	Hertzian theory, mm
10	1.7	1.4	1.9	2.5	2	2.8	2.6	1.8	2.5	1.3
15	1.8	1.6	1.9	2.7	2.1	2.3	2.7	1.9	2.6	1.5
20	2.8	2.4	2.4	2.9	2	2.7	2.8	2	2.7	1.6

4.2 Oil film thickness

The spring model (Equation (6)) was used to calculate oil film thickness from reflection coefficient. Figures 13 and 14 show the oil film thickness under varying testing conditions from sensors s2 and 4. It can be seen that the oil film formed at the contact has a V-shape, with the thinnest layer occurring at the centre of the contact, where the pressure is highest. In sliding, the entrainment speed pushed the wedge formed between the seal section profile and lower plate, dragged lubricant oil into contact and built up the pressure in the oil. Due to low moduli of the seal material, deformation on the rubber ring occurred in this process and an isoviscous EHL contact was formed. Gasni et al studied the isoviscous EHL contact between rubber ball and Perspex plate and found the minimum film thickness to be 2-5 μm when subjected to 8.9-590 mm/s sliding speed under normal load of 3.8 N [35]. Unlike the bowl-like film profile from circular point contacts [45], the oil film formed between the rubber O-ring and the concave cast-iron plate presented a symmetric V-shape with a minimum film

thickness 2.01 – 5.8 µm under 10 – 20 N loads. In all cases the film thickness is larger than the surface roughness and so full film lubrication is expected.
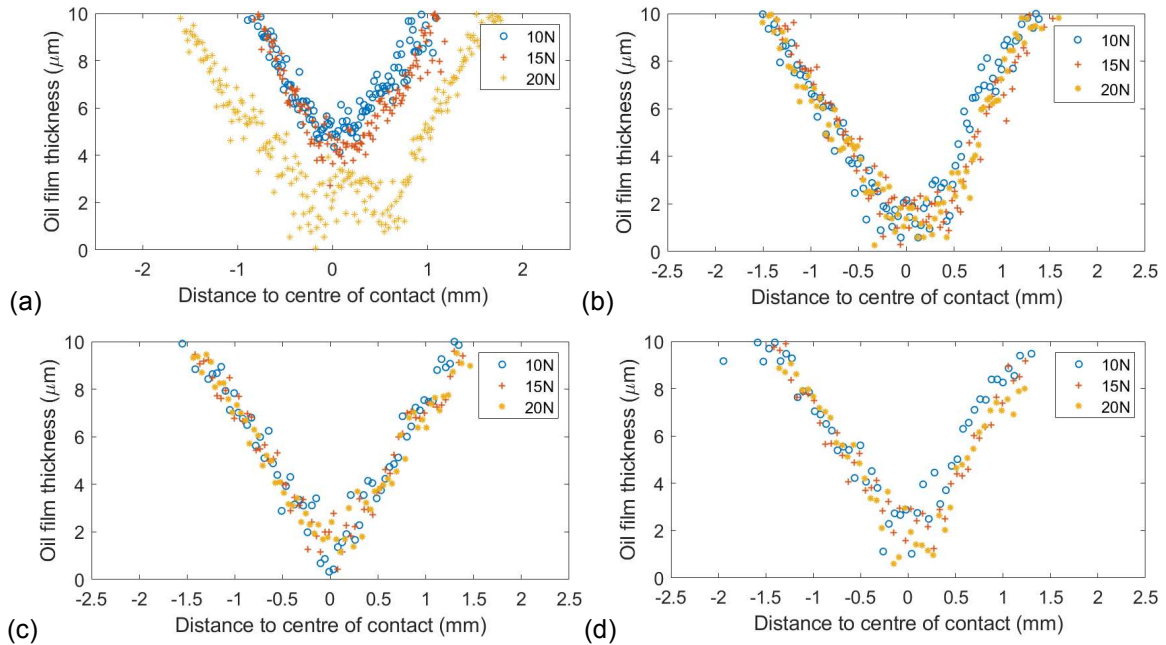
Figure 13. Oil film thickness calculated from the ultrasound reflection coefficient using the spring model under normal loads, 10, 15 and 20 N and varying reciprocating speeds (a) 2 Hz, (b) 4 Hz, (c) 6 Hz, and (d) 8 Hz, measured by ultrasound sensor s4 (middle).
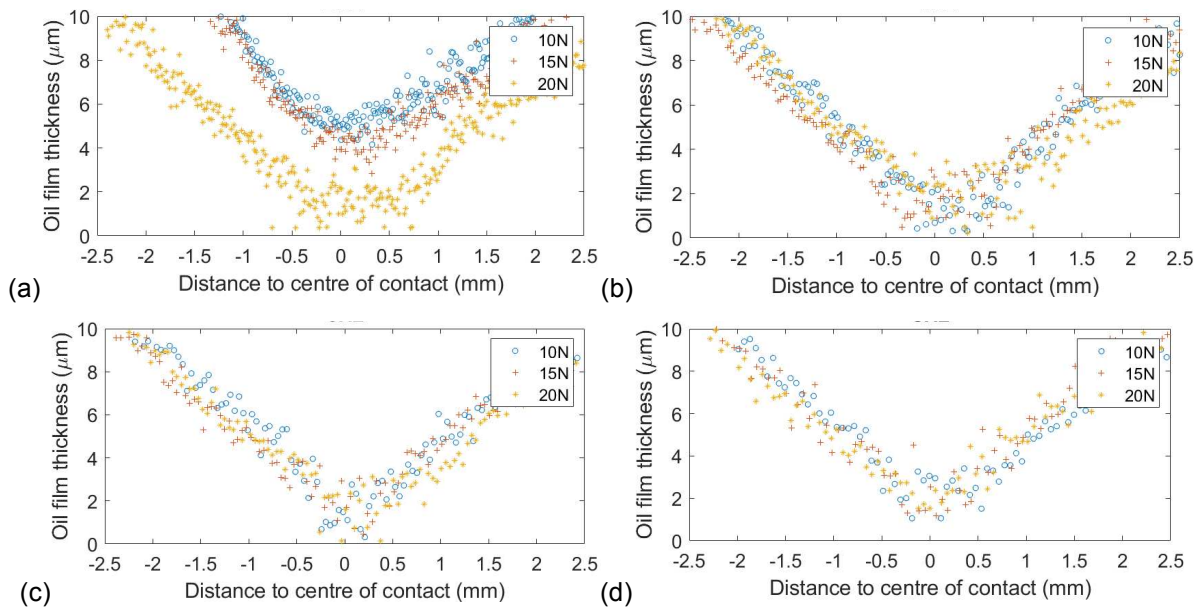
Figure 14. Oil film thickness calculated from the ultrasound reflection coefficient using the spring model under normal loads, 10, 15 and 20 N and varying reciprocating speeds (a) 2 Hz, (b) 4 Hz, (c) 6 Hz, and (d) 8 Hz, measured by ultrasound sensor s2 (edge).

Figure 15 shows the contact pressure distribution and contact width compared with oil film thickness profiles. The central oil film thickness showed the lowest value across the contact zone where the peak contact pressure of 1.31 MPa from Hertzian theory occurs. Oil film profiles from sliding speed of 4, 6, and 8 Hz show high similarity except 2 Hz which presents a higher central film thickness and smaller contact size.
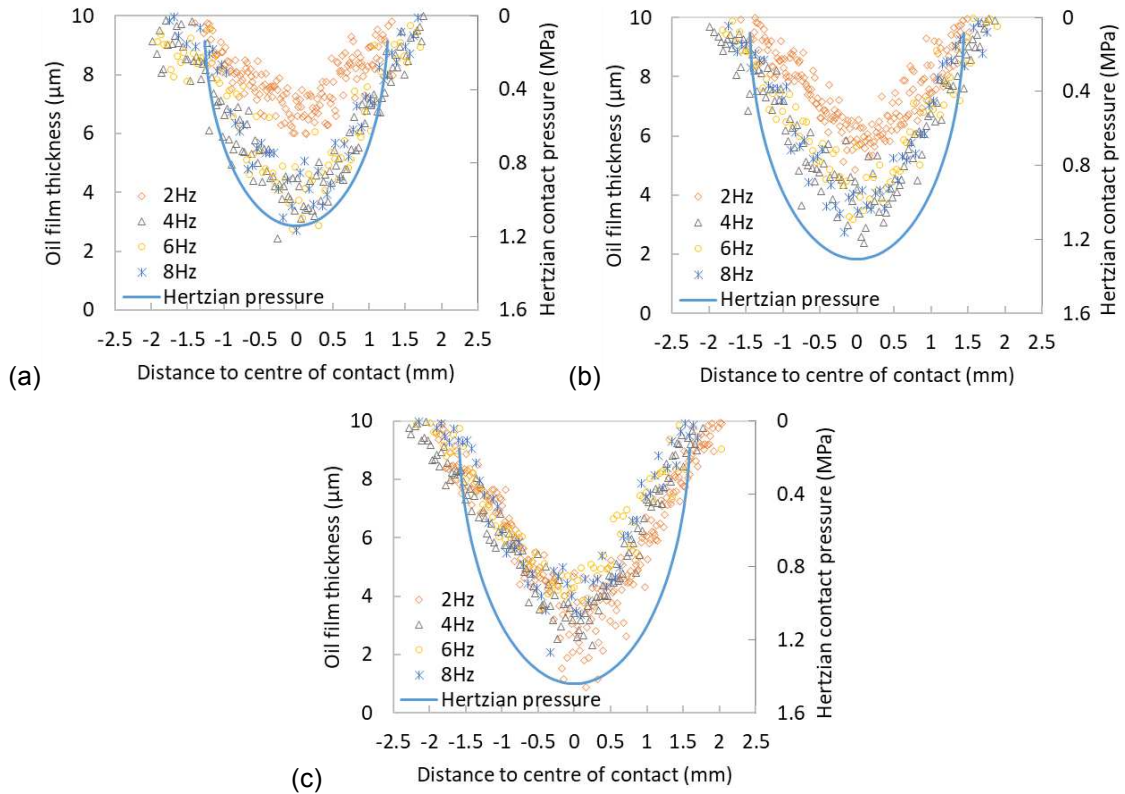
Figure 15. Hertzian pressure distribution and oil film thickness in the contact zone under normal loads, (a) 10, (b) 15, and (c) 20 N at varying reciprocating speeds measured by ultrasound sensor s6 (edge).

The central (minimum) film thickness from the preceding data has been extracted by averaging the oil thickness from the centre of the contact (contact width -0.5 to 0.5 mm) and plotted against load and speed on Figure 16. As sliding speed increases, the central film thickness starts from a relatively high value at 2 Hz, drops to around 2 μm at 4 Hz and slightly increases with speed until 8 Hz. It is interesting to note that the film thickness is not strongly affected by load (see Equations (1)-(3)); this is a typical feature of EHL also shown in [35].
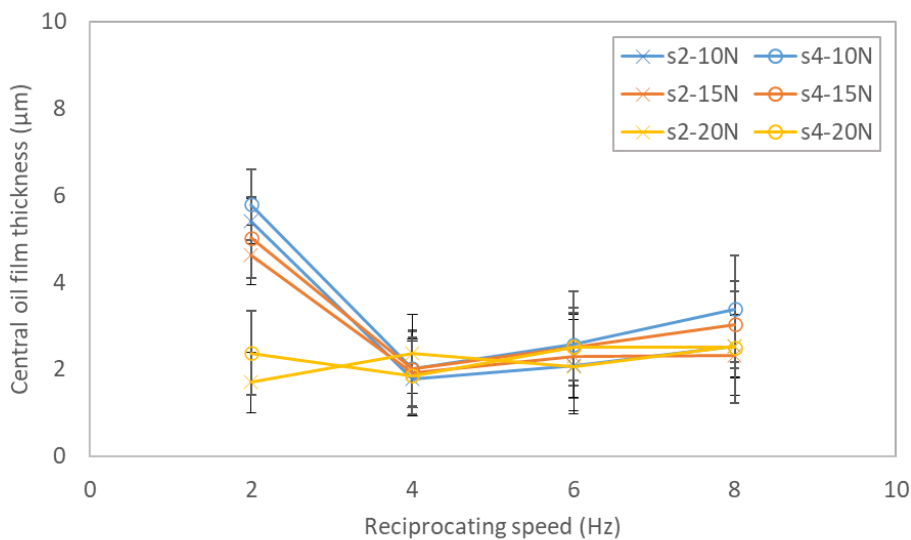
Figure 16. Central oil film thickness under varying reciprocating speeds from s2 (edge) and 4 (middle).

4.3 Comparison with model

Both the Hamrock & Dowson model and Nijenbanning et al. model were used for the prediction of the central oil film thickness for this configuration. Table 4 summarizes the comparison.

Table 4. Measured and modelling central oil film thickness (OFT).

OFT, µm	2Hz			4Hz			6Hz			8Hz		
	10N	15N	20N	10N	15N	20N	10N	15N	20N	10N	15N	20N
s2 (edge)	5.41 ±0.51	4.62 ±0.69	1.70 ±0.69	1.78 ±0.86	1.91 ±0.80	2.35 ±0.92	2.09 ±1.05	2.30 ±0.97	2.07 ±1.09	2.52 ±0.72	2.32 ±0.93	2.54 ±0.72
s4 (middle)	5.80 ±0.82	5.02 ±0.93	2.37 ±0.97	2.02 ±0.86	2.00 ±0.89	1.85 ±0.88	2.57 ±1.23	2.51 ±0.9	2.51 ±0.78	3.39 ±1.23	3.03 ±1.00	2.50 ±1.28
s6 (edge)	7.04 ±0.57	6.27 ±0.55	3.61 ±1.07	4.17 ±0.69	4.14 ±0.88	3.70 ±0.70	4.47 ±0.89	4.48 ±0.72	4.54 ±0.47	4.32 ±0.83	3.96 ±0.65	4.18 ±0.73
H&D model	3.60	3.30	3.09	5.61	5.14	4.82	7.28	6.66	6.25	8.75	8.00	7.51
Nijenbanning et al. model	4.39	4.16	4.00	6.50	6.16	5.92	8.18	7.75	7.46	9.62	9.12	8.77

At higher reciprocating speeds, the model predicts thicker oil layers in the center of the contact, which are comparable to the measurements. The trends broadly agree, except for the case of 2Hz. It is not clear why the film thickness at lowest frequency is thicker than the model predicts, and indeed thicker than at higher frequencies when the entraining speed is higher.

Figure 17 shows the central oil film thickness varying against the product of dimensionless load and speed parameters, $\frac{\eta_0 \times u_s}{E' \times R'_x} \cdot \frac{P}{E' \times R'^2_x}$. For comparison, oil film thicknesses from a PDMS (Polydimethylsiloxane) ball sliding against glass prism [45] using the optical interference and laser induced fluorescence techniques, and from a nitrile ball sliding against Perspex [35] using the ultrasound technique are over-plotted.
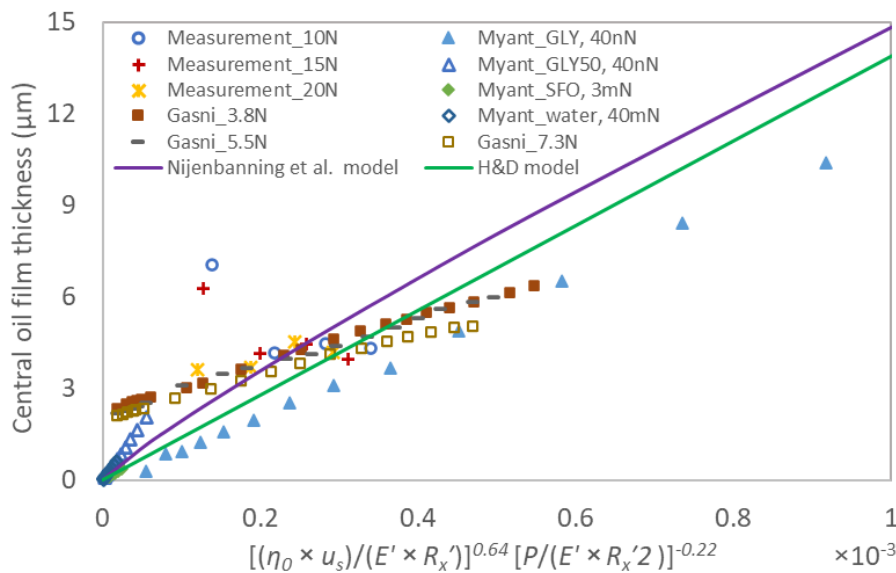
Figure 17. Comparison of central oil film thickness from s6 with modelling (Nijenbanning et al. model and H&D model), and experimental results from Myant [45] (GLY: glycerol, GLY50: 50% wt. glycerol solution in distilled water, SFO: sunflower oil) and Gasni et al. [35]

In the theoretical simulation, perfectly smooth contacting surfaces are assumed which makes an extremely thin layer possible. However, in the real sealing contact, due to surface roughness, the central film thickness can be in the order of the surface roughness especially under low speeds and/or high loads. In this case, rough asperity contact occurs which affects the ultrasound reflection and hence measured oil thickness. This possibly explains the mismatch between model prediction and the actual measurements when the reciprocating speed is 2 Hz shown in Figure 17.

When looking at the modelling parameters, the current testing conditions produce dimensionless speed and load parameters, $\overline{U}$ and $\overline{W}$, out of the range from the empirical fits of the theoretical model. For example, the Hamrock and Dowson's model was fitted to a range of $\overline{U}$: 0.5 - 5.1 × 10^{-6}, and $\overline{W}$: 0.2 - 2.2 × 10^{-3}, while the values in this work are $\overline{U}$: 0.6 - 2.3 × 10^{-5}, and $\overline{W}$: 1.7 - 3.4. The accuracy of the theoretical modelling seems to rely more on the testing conditions and contact configurations.

4.4 Film thickness footprint

Figure 18-21 show film thickness maps in the contact zone measured by each of the five sensors against reciprocation sliding time. Along the stroke distance, the seal was sliding over sensors 2 to 6 and reversing; in each plot two complete cycles are shown. In each measured region, oil layer showed the thinnest film in the contact center, corresponding to the maximum contact pressure region. Overall, there was no significant correlation between reciprocating speeds, normal loads, and the detected oil film thickness except at the lower speed, 2 Hz (Figure 18), a thinner oil film was observed for higher loads.
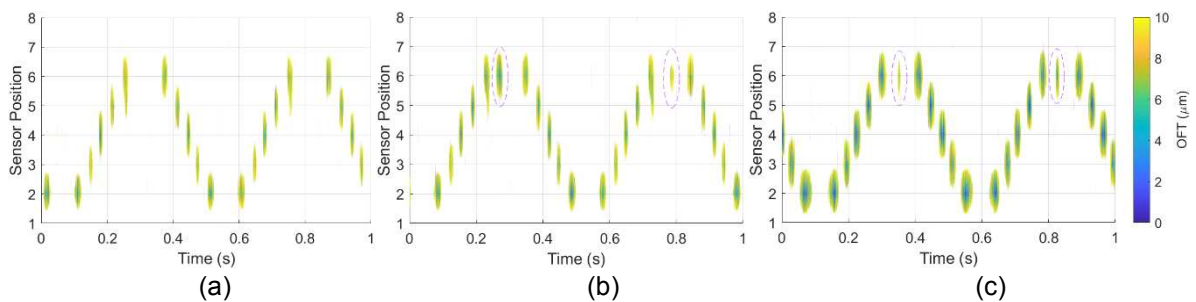
Figure 18. Oil film thickness footprint in sliding from ultrasound sensors at 2Hz reciprocating speed under normal loads, (a) 10N, (b) 15N, and (c) 20N.
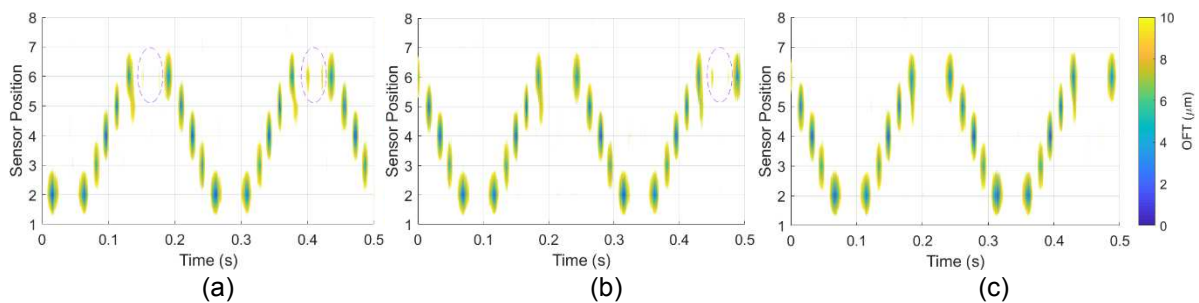
Figure 19. Oil film thickness footprint in sliding from ultrasound sensors at 4 Hz reciprocating speed under normal loads, (a) 10 N, (b) 15 N, and (c) 20 N.
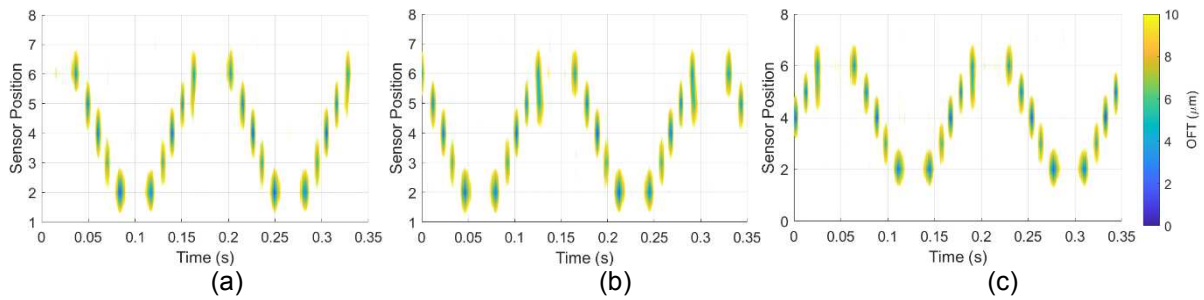
Figure 20. Oil film thickness footprint in sliding from ultrasound sensors at 6 Hz reciprocating speed under normal loads, (a) 10 N, (b) 15 N, and (c) 20 N.
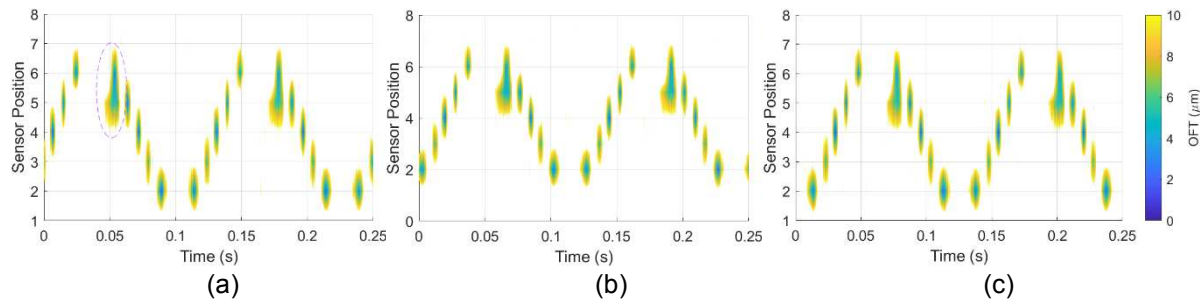
Figure 21. Oil film thickness footprint in sliding from ultrasound sensors at 8Hz reciprocating speed under normal loads, (a) 10 N, (b) 15 N, and (c) 20 N.

As highlighted in Figures 18 (c) and 19 (c), a small area of 'film footprint' was detected by the sensor 6 when the rubber ring slid over the stroke end and reversed. A disturbance may have occurred to the contact which caused the change in the ultrasound reflection. This fast transitionary process maybe caused by stick-slip at the rubber-metal contact, especially under the high loads and low speeds, 2 Hz and 4 Hz (Figures 18 (c) and 19 (c)). Ogata et al [46] studied the oil film formation for lip-type oil seals subject to a wide range of speeds (0.003 m/s to 18 m/s) and concluded a stick-slip process occurred in the sealing contact at speeds lower than 0.18 m/s. It was claimed that under extreme slow speed, dry friction took place which induced the stick-slip. This also explains the blurring zone highlighted in Figure 21. On the return of the stroke, as the sliding direction changed, the speed approached to zero. This extremely low speed promoted the development of stick at the interface. A wider contact zone was therefore caused and detected by sensor 5. Due to the sparse allocation of the sensors, the process of the film formation and break down during stick-slip transition was not fully assessed. There was no stick-slip process observed in the middle of the stroke where normal 'faster' reciprocating speeds take place.

5. Conclusions

An elastomer seal contact between a nitrile rubber O-ring section and a concave cast-iron plate, lubricated by Shell Helix HX5 15W-40 oil, was designed for reproducing the isoviscous-EHL contact of a hydraulic reciprocating seal. The reciprocating motion was created using the versatile tribometer, Plint TE 77, subjected to varying sliding speeds and normal loads. The formation of oil films and their distributions were studied using an ultrasound technique by recording the ultrasound reflection from the contact zone. Theoretical models were used for predicting the oil film thickness which was compared with experimental observations. Conclusions from the work are summarized as follows:

- The ultrasound method was developed and applied for assessing the reciprocating sealing contact. A sensor array mounted on the cast-iron plate covered the reciprocating distance of the seal. The ultrasound reflection coefficient was found to

be in the range of 0.87 - 1 from the sealing contact zone. Lower loads and higher speeds produce lower ultrasound reflection due to thicker oil layers.

- Oil film thickness was calculated from the ultrasound reflection coefficient using the spring model. In the middle of the contact zone, a thinner oil film was observed. This central oil film thickness was in the range of 1.8 – 7 µm while higher normal loads lead to a thinner oil layer.

- The contact width was predicted using the Hertzian theory, which showed a good agreement with the ultrasound measurements represented by the ultrasound reflection from the contact zone.

- Modeling of the oil film thickness in the center of the contact was conducted. Theoretical simulations and experimental measurements showed a good agreement for the higher speed cases, 4-8 Hz.

- Oil film formation along the reciprocating distance was mapped by the ultrasound measurements. Higher normal loads produced a greater contact zone. When the seal approached the end of the stroke length, stick-slip was observed as detected by the ultrasound reflections.

Acknowledgments

References

[1] Wang J, Li Y, Lian Z. Numerical Investigations on the Sealing Performance of a Reciprocating Seal Based on the Inverse Lubrication Method. ASME Journal of Tribology. 2019; 141: 112201.
[2] Peng C, Guo S, Ouyang X, Zhou Q, Yang H. An eccentric 3-D fluid-structure interaction model for investigating the effects of rod parallel offset on reciprocating-seal performance. Tribology International. 2018; 128: 279-290.
[3] Nikas GK. Research on the tribology of hydraulic reciprocating seals. In Tribology research trends (Ed. T. Hasegawa). Nova Science Publishers, New York, USA. 2008.
[4] Nikas GK. Eighty years of research on hydraulic reciprocating seals: review of tribological studies and related topics since the 1930s. Proceedings of the Institution of Mechanical Engineers, Part J: Journal of Engineering Tribology. 2010; 224(1):1-23.
[5] Denny DF. The friction of rubber sealing rings. British Hydromechanics Research Association, Res. report No. 458, Harlow, UK. 1953.
[6] Denny DF. The lubrication of fluid seals. In Proceedings of the IMechE Conference on Lubrication and Wear. London, UK. 1957.
[7] Denny DF. Leakage characteristics of rubber seals fitted to reciprocating shafts. In Proceedings of the IMechE Symposium on Oil Hydraulic Power Transmission and Control, London, UK. 1961; 259-268.
[8] Prati E, Strozzi A. A study on the elastohydrodynamic problem in rectangular, elastomeric seals. ASME Journal of Tribology. 1984; 106(4): 505-512.
[9] van Leeuwen H, Petterson R, Meesters K. Cinderella in fluid film lubrication: stretch effects in radial lip seals. The 38th Leeds–Lyon Symposium on Tribology: Energy and Health. Villeurbanne, Franc. 2011.
[10] van Leeuwen H, Wolfert M, The sealing and lubrication principles of plain radial lip seals: an experimental study of local tangential deformations and film thickness. Editor(s): Dowson D, Taylor CM, Childs THC, Dalmaz G, Berthier Y, Flamand L, Georges JM, Lubrecht AA. Tribology Series. Elsevier., 1997; 32:219-232.

[11] Crudu M, Fatu A, Cananau S, Hajjam M, Pascu A, Cristescu C. A numerical and experimental friction analysis of reciprocating hydraulic 'U'rod seals. Proceedings of the Institution of Mechanical Engineers, Part J: Journal of Engineering Tribology. 2012; 226(9): 785-794.

[12] Liao C, Suo S, Wang Y, Huang W, Liu Y. Study on stick–slip friction of reciprocating o-ring seals using acoustic emission techniques. Tribology Transactions. 2012; 55(1): 43-51.

[13] Rana AS, Sayles RS. An experimental study on the friction behaviour of aircraft hydraulic actuator elastomeric reciprocating seals. Tribology and Interface Engineering Series. 2005; 48: 507-515.

[14] Rana AS, Sayles RS, Nikas GK, Jalisi I. An experimental technique for investigating the sealing principles of reciprocating elastomeric seals for use in linear hydraulic actuator assemblies. Proceedings of the 2nd world tribology congress, Vienna, Austria, September 2001.

[15] Nikas GK, Almond RV, Burridge G. Experimental study of leakage and friction of rectangular, elastomeric hydraulic seals for reciprocating motion from −54 to +135 °C and pressures from 3.4 to 34.5 MPa. Tribology Transactions. 2014; 57(5): 846-865.

[16] Chen P, Chua P, Lim G. An experimental study of monitoring internal leakage in water hydraulic cylinders using acoustic emission. Journal of Testing and Evaluation. 2005; 33(6): 445-451.

[17] Field GJ, Nau BS. An experimental study of reciprocating rubber seals. In Proceedings of the IMechE Symposium on Elastohydrodynamic Lubrication, Leeds, UK. 1972; 29-36.

[18] Field GJ, Nau BS. The effects of design parameters on the lubrication of reciprocating rubber seals. In Proceedings of the 7th International Conference on Fluid sealing, Nottingham, UK. 1975; 1-13.

[19] Hirano F, Kaneta M. Experimental investigation of friction and sealing characteristics of flexible seals for reciprocating motion. In Proceedings of the 5th International Conference on Fluid sealing, Coventry, UK. 1971; 33-48.

[20] Field GJ. The elastohydrodynamic lubrication of rectangular section rubber seals under conditions of reciprocating motion. PhD Thesis, City University London, England, 1973.

[21] Shanbhag VV, Meyer TJJ, Caspers LW, Schlanbusch R. Condition monitoring of hydraulic cylinder seals using acoustic emissions. International Journal of Advanced Manufacturing Technology. 2020; 109:1727-1739.

[22] Kanzaki Y, Kawahara Y, Kaneta M. Optical interferometric observations of oil film behaviour in reciprocating rubber seals. Transactions of the Japan Society of Mechanical Engineers, Part C. 1996; 62(600): 3229-3236.

[23] Kanzaki Y, Kawahara Y, Kaneta M. Oil film behaviour and friction characteristics in reciprocating rubber seals. Part 1: single contact. Proceedings of the 15th International Conference on Fluid sealing. Maastricht, the Netherlands. 1997; 79-95.

[24] Blok, H, Koens HJ. The breathing film between a flexible seal and a reciprocating rod. Proceedings of the Institution of Mechanical Engineers, Conference Proceedings. 1965/66; 180(part 3B): 221-223.

[25] Rana AS. A tribological study of elastomeric reciprocating seals for hydraulic actuators. PhD Thesis, Imperial College London, 2005.

[26] Claus RG. Development of a high performance, heavy duty piston seal. The 49th National Conference on Fluid Power. Las Vegas, USA. 2002.

[27] Nikas GK, Sayles RS. Study of leakage and friction of flexible seals for steady motion via a numerical approximation method. Tribology International. 2006; 39(9):921-936.

[28] Dwyer-Joyce RS, Harper P, Drinkwater B. A Method for the Measurement of Hydrodynamic Oil Films Using Ultrasonic Reflection. Tribology Letters. 2004; 17:337-348.

[29] Dwyer-Joyce RS, Reddyhoff T, Zhu J. Ultrasonic measurement for film thickness and solid contact in elastohydrodynamic lubrication, ASME Journal of Tribology. 2011; 133(3):031501.

[30] Kendall K, Tabor D. An Ultrasonic Study of the Area of Contact between Stationary and Sliding Surfaces. Proceedings of the Royal Society A: Mathematical, Physical and Engineering Sciences. 1971; 323:321-340.

[31] Zhu J, Pugh S, Dwyer-Joyce RS, Beke A, Cumner G, Ellaway T. Experiments on the pressure distribution and frictional torque in articulating pin joints. Proceedings of the Institution of Mechanical Engineers, Part J: Engineering Tribology. 2010; 224(10):1153-1162.

[32] Li X, Dwyer-Joyce RS. Measuring friction at an interface using ultrasonic response. Proceedings of the Royal Society A: Mathematical, Physical and Engineering Sciences. 2020; 476 (2241): 20200283.

[33] Reddyhoff T, Dwyer-Joyce RS. Ultrasonic measurement of film thickness in mechanical seals. Sealing Technology. 2006; 2006(7):7-11.

[34] Reddyhoff T, Dwyer-Joyce RS, Harper P. A new approach for the measurement of film thickness in liquid face seals. Tribology Transactions. 2008; 51(2):140-149.

[35] Gasni D, Wan Ibrahim MK, Dwyer-Joyce RS. Measurements of lubricant film thickness in the iso-viscous elastohydrodynamic regime. Tribology International. 2011; 44(7–8):933-944.

[36] Fowell MT, Myant C, Spikes HA, Kadiric A. A study of lubricant film thickness in compliant contacts of elastomeric seal materials using a laser induced fluorescence technique. Tribology International. 2014; 80:76-89.

[37] Kumar R, Azam MS, Ghosh SK, Yadav S. 70 years of Elastohydrodynamic Lubrication (EHL): A Review on Experimental Techniques for Film Thickness and Pressure Measurement. Journal of Metrology Society of India. 2018; 33:481-491.

[38] Albahrani S, Philippon D, Vergne P, Bluet J. A review of in situ methodologies for studying elastohydrodynamic lubrication. Proceedings of the Institution of Mechanical Engineers, Part J: Journal of Engineering Tribology. 2016; 230(1):86-110.

[39] Hamrock BJ, Dowson D. Elastohydrodynamic lubrication of elliptical contacts for materials of low elastic modulus i—fully flooded conjunction. ASME Journal of Lubrication Technology. 1978; 100(2): 236-245.

[40] Kanters AFC. On the calculation of leakage and friction of reciprocating elastomeric seals. PhD Thesis. Technische Universiteit Eindhoven. Netherlands. 1990.

[41] Crook AW. The lubrication of rollers - II. Film thickness with relation to viscosity and speed. Philosophical Transactions of the Royal Society of London. Series A, Mathematical and Physical Sciences. 1961; 254:223-258.

[42] Nijenbanning G, Venner CH, Moes H. Film thickness in elastohydrodynamically lubricated elliptic contacts. Wear. 1994; 176(2):217-229.

[43] Moes H. Optimum similarity analysis with applications to elastohydrodynamic lubrication. Wear. 1992; I59:56-66.

[44] Tattersall HG, The ultrasonic pulse-echo technique as applied to adhesion testing. Journal of Physics D: Applied Physics. 1973; 6(7):819-832.

[45] Myant C. Experimental techniques for investigating lubricated, compliant, contacts. PhD Thesis. Imperial College London. 2010.

[46] Ogata M, Fujii T, Shimotsuma Y, Paper XVIII(ii) Study on fundamental characteristics of rotating lip-type oil seals. Editor(s): Dowson D, Taylor CM, Godet M, Berthe D. Tribology Series. Elsevier. 1987; 11:553-560.